CHEMICAL ENGINEERING TRANSACTIONS
VOL. 116, 2025
A publication of AIDIC
The Italian Association of Chemical Engineering
Online at www.cetjournal.it
Guest Editors: Bruno Fabiano, Valerio Cozzani

ISBN 979-12-81206-18-2; **ISSN** 2283-9216
DOI: 10.3303/CET25116036

Safety Assessment of MLI Super-Insulation Systems for Cryogenic Liquid-Hydrogen Tanks in Fire Scenarios

Davide Camplese[a,*], Chiara Cozzolino[a], Giordano Emrys Scarponi[a], Robert Eberwein[b], Frank Otremba[b], Valerio Cozzani[a]

[a]Alma Mater Studiorum - Università di Bologna, Dipartimento di Ingegneria Civile, Chimica, Ambientale e dei Materiali, via Terracini 28, 40131 Bologna, Italy
[b]Bundesanstalt für Materialforschung und -prüfung (BAM), Berlin
davide.camplese@unibo.it

In the context of green energy transition, cryogenic tanks insulated by MLI and vacuum are emerging as a leading solution to store hydrogen in heavy-duty vehicles. However, the integrity of such tanks can be jeopardized by fire. In such a scenario, MLI materials degradation can occur, leaving the tank unprotected from the fire heat flux, with consequent rapid pressurization and a high risk of failure. This study presents a safety assessment of non-combustible MLI under fire exposure based on the estimation of the time to mechanical failure of the equipment. This is calculated through an innovative model that simulates the thermomechanical response of the tank, including the MLI thermal degradation and the pressure-relief valve (PRV) operation. The application to several case studies that consider a typical LH_2 tank featuring a wide range of MLI configurations demonstrated the likelihood of failure in case of exposure to a hydrocarbon pool fire, providing also comprehensive insights into the impact of the insulation characteristics and operating conditions on the time to failure.

1. Introduction

Within the energy transition scenario, hydrogen is widely recognized as a promising alternative to conventional fuels due to its minimal environmental impact (Preuster et al., 2017). Among its storage solutions, liquefied hydrogen (LH_2) in cryogenic tanks featuring multilayer insulation (MLI) is particularly effective for hydrogen-powered applications as it provides high volumetric energy density (Kunze and Kircher, 2012). MLIs consist of multiple thin foils (typically 20 to 80) of highly reflective material, referred to as reflective layers, separated by spacers with low thermal conductivity. These are housed within the double-walled shell of the tank, working under high-vacuum conditions. Due to lower volume requirements compared to other insulation materials, MLI systems are among the most widely adopted insulation technologies in the transportation sector, where space and weight are critical constraints (Edward and Filip, 2018). Although the large-scale adoption of LH_2 storage and transportation technologies offers widely recognized advantages, this also poses several hazards due to the high flammability of hydrogen (Schiaroli et al., 2024). Accidental releases may trigger dangerous events, such as flash fires, vapor cloud explosions, and jet fires. Real-scale fire tests (van Wingerden et al., 2022) showed that, despite the presence of an MLI system, Boiling Liquid Expanding Vapour Explosions (BLEVEs) and fireballs may result from the catastrophic failure of the tank upon exposure to external fire. This was attributed to insulation degradation, as further confirmed by Eberwein et al. (2024a), who showed that high temperatures can severely damage MLI, directly exposing the tank lading to the fire heat flux. This results in pressurization and temperature increases that weaken the tank wall, posing a serious threat to structural integrity. In this framework, reliable and robust tools to assess the thermal response of the tank under fire scenarios and quantify how much this can be influenced by MLI system configuration are crucial to enhance the safety of LH_2-powered new technologies and improve emergency response planning. This study proposes an innovative safety assessment of LH_2 tanks equipped with MLIs based on the time to failure (TTF) estimation of the equipment through an advanced modeling approach. The model developed for this innovative safety

Paper Received: 29 November 2024; Revised: 9 February 2025; Accepted: 25 March 2025
Please cite this article as: Camplese D., Cozzolino C., Scarponi G.E., Eberwein R., Otremba F., Cozzani V., 2025, Safety Assessment of Mli Super-insulation Systems for Cryogenic Liquid-hydrogen Tanks in Fire Scenarios, Chemical Engineering Transactions, 116, 211-216 DOI:10.3303/CET25116036

assessment calculates the tank heating up and pressurization resulting from fire exposure, accounting for the degradation of the MLIs performances induced by high temperatures and for the action of the pressure relief valve (PRV). The TTF is estimated by including in the model a simplified mechanical stress analysis of the tank. The proposed approach was applied to a set of case studies addressing a vehicle-scale LH_2 tank featuring aluminum-based MLI at various layer numbers and pressures within the insulation to assess their impact on the TTF under a typical hydrocarbon-pool fire scenario defined by standards. The results provide valuable information to support the safe design of MLI-equipped LH_2 tanks and emergency management in case of fire.

2. Methodology

The methodology for the innovative fire safety assessment of the typical aluminum-based MLI insulation systems for LH_2 tanks is divided into three stages. The first one (Section 2.1) is devoted to the definition of the analytical model to calculate the thermodynamic response of these tanks to fire in terms of pressure and temperature. The second one (Section 2.2) describes the failure model adopted to calculate the TTF. Finally, the third stage (Section 2.3) defines the case studies considered for the analysis.

2.1 Model definition

The approach developed to predict the response of the tank under fire exposure consists of two sub-models described in the following: the first one is devoted to the simulation of the thermodynamic behavior of the tank lading, while the second one calculated the heat flux through the MLI accounting for its thermal degradation.

Table 1. Set of the equation used in the LH_2 thermodynamic model.

Node	Variable	Equation	Eq. N°
H_2	m_{H2}	$\frac{dm_{H2}}{dt} = -\phi \dot{m}_{PRV}$	(1)
H_2	U_{H2}	$\frac{dm_{H2}\hat{U}_{H2}}{dt} = q_{H2}A_S - \phi \dot{m}_{PRV}\hat{H}_{PRV}$	(2)
-	ϕ [b]	$\phi = \begin{cases} 1, & PRV\ open \\ 0, & PRV\ close \end{cases}$	(3)
-	$\dot{m}_{PRV}$ [a]	$\dot{m}_{PRV} = \begin{cases} K_{dr}A_{PRV}\sqrt{\gamma\rho P\left(\frac{2}{\gamma+1}\right)^{\left(\frac{\gamma+1}{\gamma-1}\right)}}, & \frac{P_o}{P} \le \left(\frac{2}{\gamma+1}\right)^{\left(\frac{\gamma}{\gamma-1}\right)} \\ K_{dr}A_{PRV}\sqrt{\gamma\rho P\left(\frac{2}{\gamma-1}\right)\left[\left(\frac{P_o}{P}\right)^{2/\gamma} - \left(\frac{P_o}{P}\right)^{(\gamma+1)/\gamma}\right]}, & \frac{P_o}{P} > \left(\frac{2}{\gamma+1}\right)^{\left(\frac{\gamma}{\gamma-1}\right)} \end{cases}$	(4)
-	q_{H2}	$q_{H2} = h(T_{Si} - T_{H2})$	(5)
-	h	$h = (h_L A_L + h_V A_V)/A_S$	(6)

[a] K_{dr} is the discharge coefficient of the PRV (assumed equal to 0.82, ISO 21013-3:2016); γ is the specific heat capacity ratio (1.41); ρ is the density of the discharging mass flow (kg/m^3); P_o is the pressure at the outlet of the PRV (10^5 Pa); A_{PRV} is the cross sectional area of the PRV (m^2).

[b] PRV remains closed until the pressure reaches $P_{PRV,open}$, and it remains so until the pressure below $P_{PRV,close}$

A single-zone lumped equilibrium model is used to calculate the pressurization and temperature increase within the tank. The fluid domain is represented by a single thermal node (*H2*; see Figure 1), for which mass and thermal balances are written (see Eqs. (1) and (2) in Table 1) assuming thermodynamic equilibrium between the liquid and gaseous hydrogen phases (i.e., they share the same temperature, T_{H2}). Both balance equations account for the effect of the pressure relief valve (PRV) through an activation factor, ϕ, which is 0 when the valve is closed and 1 when open. The discharging mass flow and enthalpy ($\dot{m}_{PRV}$, and $\hat{H}_{PRV}$, respectively), are calculated using Eq. (4) (Van Den Bosh and Weterings, 2005), assuming a vapor fraction of 1 in the outlet stream. The heat flux term q_{H2} in the energy balance (Eq. (2), Table 3) represents the heat transfer from the inner shell and is calculated using Eq. (6) (Table 3). Here, A_S and h represent the inner shell area and the heat transfer coefficient of the fluid in contact with the wall, respectively. h is determined by Eq. (6) (Table 1) as the area-weighted average value between the liquid hydrogen boiling heat transfer coefficient (h_L) and the vapor-wall convective heat transfer coefficient (h_V). The value of h_L is estimated from correlations by Wang et al.

(2016) for different regions of the boiling curve, while h_V is retrieved from Churchill and Usagi, (1972). These coefficients are weighted by the tank wall surface areas in contact with liquid (A_L) and vapor (A_V) phases, respectively. Hydrogen thermodynamic properties are obtained from the "CoolProp" database (Bell et al., 2014). After determining the specific internal energy ($\hat{U}_{H2}$) and the hydrogen mass (m_{H2}) from the energy and mass balances, the tank pressure (P) is calculated based on an equation of state specifically developed for hydrogen and implemented in the database. The fire boundary condition is defined assuming a full engulfment scenario. The heat flux entering the external wall of the thank, q_f, is computed at each time step according to Eqs. (8) to (10), where $q_{rad,f}$ and $q_{conv,f}$ represent the fire radiative and convective heat fluxes, ε_f is the flame emissivity (here assumed equal to 1), T_f and T_{Se} are the flame and external shell temperatures, $\varepsilon_{Se,out}$ is the emissivity of the external wall on the side facing the fire (here assumed equal to 0.9), h_f is the fire convective heat transfer coefficient (assumed as equal to 10 W·m^{-2}·K^{-1}), and σ is the Stefan-Boltzmann constant (5.67·10^{-8} W·m^{-2}·K^{-4}).

$$q_f = q_{rad,f} + q_{conv,f} \tag{7}$$

$$q_{rad,f} = \sigma \varepsilon_{Se,out} (\varepsilon_f {T_f}^4 - {T_{Se}}^4) \tag{8}$$

$$q_{conv,f} = h_f (T_f - T_{Se}) \tag{9}$$

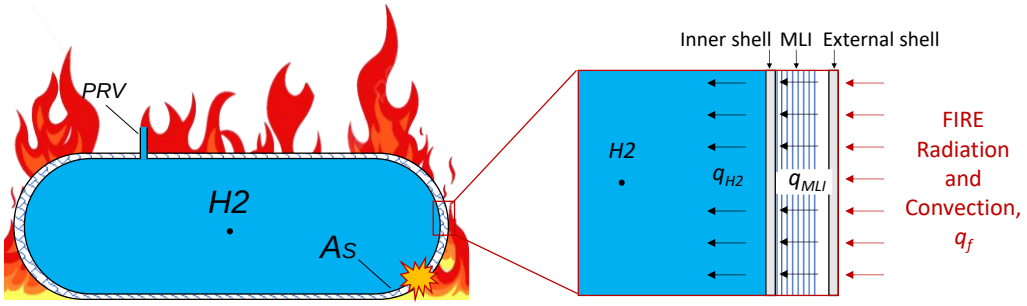

Figure 1. Schematic representation of the failure model.

The MLI heat transfer model is applied to bridge the fire boundary condition assigned at the outer wall and the heat flux that enters the inner shell of the tank. This is based on the approach proposed in previous works (Camplese et al., 2024) and it exploits a thermal node discretization in which the insulation system is divided into N+2 nodes. One node is assigned to each one of the reflective layers of the MLI, while two additional thermal nodes represent the external shell, S_e, and the inner shell, S_i, of the tank. A transient one-dimensional heat balance is written for each node and solved to obtain the temperature distribution of the insulation system and the tank shells over time. The heat balance through the MLI layers is a modified version of the well-established McIntosh classical "layer-by-layer" model (McIntosh, 1994), in which the net heat flux between any adjacent couple of layers is given by the sum of thermal radiation, spacer solid conduction, and the gas conduction/convection (depending on the vacuum pressure and fluid-dynamic regime). This allows the heat transfer model to account for vacuum losses within the insulation system. The equation system is reported and discussed in detail in Camplese et al.(2024). In the simulation of high-temperature degradation of the MLI, it is assumed that each radiation layer is fully and instantaneously destroyed upon reaching a specified degradation temperature, T_{deg} (see Section 2.3). Following this degradation, the affected layer is replaced by a vacuum gap of equivalent thickness, allowing only radiation and gas conduction/convection to occur between the first undamaged layer and the external shell, as further detailed in Camplese et al. (2024).

2.2 Failure criterion

The integrity of the tank is checked at each timestep by the Von Mises yield (maximum distortion energy) criterion. Inner vessel rupture is assumed to occur when the equivalent mechanical stress caused by pressure buildup (σ_V) equals the yield strength of the shell material (σ_y), as described by Eq. (11).

$$\sigma_V = \sigma_y \tag{11}$$

The first term (σ_V) is given by using Eq. (12), where σ_l, σ_h, and σ_r are the longitudinal, circumferential, and radial primary stresses, r and δ_{S_i} represent the inner shell radius and thickness, and P_g is the inner tank gauge

pressure. The yield strength of the shell material (σ_y) varies with the shell temperature through the strength reduction coefficients provided by EN 1993-1-2:2024.

$$\sigma_V = \sqrt{\frac{(\sigma_l-\sigma_h)^2+(\sigma_h-\sigma_r)^2+(\sigma_l-\sigma_r)^2}{2}} \quad ; \quad \sigma_l = \frac{P_g \cdot r}{2\delta_{S_i}} \quad ; \quad \sigma_h = \frac{P_g \cdot r}{\delta_{S_i}} \quad ; \quad \sigma_r = -P_g \tag{12}$$

As a conservative estimation of the TTF, the maximum inner shell temperature ($T_{Si,max}$) is used for the analysis. This is calculated by Eq. (13), neglecting the heat transferred from the shell to the fluid in the tank (i.e. q_{H2} = 0). δ_{S_i}, ρ_{Si}, $c_{p,Si}$ are the thickness, density, and the specific heat capacity of the inner shell wall, while q_{MLI} is the heat flux coming from the first intact MLI layer or the external shell wall in case MLI is completely degraded.

$$q_{MLI} = \delta_{S_i} \rho_{Si} c_{p,S_i} \frac{dT_{S_i,max}}{dt} \tag{13}$$

2.3 Case studies

The modeling approach presented in Sections 2.1 and 2.2 was applied to a set of case studies to assess the impact of MLI system properties and working conditions on the time to failure of the vessel. The tank chosen for the present study has a horizontal orientation, with an inner tank of a length of 1.75 m and a diameter of 0.55 m, resulting in a volume of 0.4 m^3. Such dimensions are representative of storage tanks used for cryogenic hydrogen-powered heavy-duty trucks. The tank is equipped with a pressure-relief valve having an opening section (A_{PRV}) of $5.1 \cdot 10^{-4}$ m^2, which opens when the pressure inside the tank reaches 4.7 bar ($P_{PRV,open}$) and closes for pressures below 4.2 bar ($P_{PRV,open}$). The tank is filled with liquid hydrogen up to 55% of the inner tank volume as in the real-scale fire test conducted by Pehr, (1996). Both the external and internal shells consist of AISI 316L, each having a thickness of 0.002 m. The tanks featured a typical commercial uniform-density MLI composed of pure aluminum reflective layers and glass fiber fleece spacers. The vacuum gap has a thickness of 0.05 m and air is considered as the residual gas. The degradation temperature (T_{deg}) was defined as 660 °C (i.e.. the melting point of aluminum). All the other data needed to close the model set of equations for the specific MLI considered are assumed from previous works and can be found elsewhere (Camplese et al., 2024). In each simulation run, the MLI parameters were kept constant except for the number of layers (N), which ranged from 20 to 80 to encompass typical commercial applications, and the pressure within the insulation system, which varied between 0.001 Pa (representative of typical high-vacuum conditions) and atmospheric value. It is worth mentioning that the value of pressure within the MLI system has a critical impact on the insulation performance at room temperatures (Edward and Filip, 2018), as loss of vacuum has been demonstrated to reduce the insulation effectiveness by a factor of 100 and 1000 times compared to high-vacuum. Such vacuum loss is to occur in fire scenarios (van Wingerden et al., 2022); however, its direct impact on insulation properties in these conditions has been scarcely investigated in the past. The reference scenario selected for the analysis is a full engulfment pool fire, with a flame temperature (T_f) defined through a standard hydrocarbon flame curve (EN 1993-1-4:2006). This presents a maximum flame temperature of 1100°C. The initial temperature profile at each node reflects the steady-state solution derived from constant boundary temperatures: a liquid temperature of -252.75 °C, an outer shell temperature of 25 °C, and high-vacuum pressure within the MLI system (i.e., 0.001 Pa). This setup represents the system condition before exposure to fire. At t=0 s fire is ignited and the simulation runs up to the minimum value between TTF and 60 min, with a timestep of 0.05 s.

3. Results and discussion

Figure 2a presents the estimated time to failure (TTF) as a function of the number of MLI layers and the working pressure within the insulation system. In the specific fire scenario under investigation, mechanical failure of the tank occurred for all the MLI configurations considered, showing that intense fire conditions can severely threaten the integrity of MLI-equipped LH_2 tanks. Increasing the number of layers has a limited beneficial effect on TTF, with failure delayed by 1 min 40 s to 3 min regarding 80 layers compared to 20 layers, at a constant insulation pressure. On the contrary, the insulation pressure has a substantial impact on TTF: shifting from high-vacuum (i.e., 0.001, 0.1, and 1 Pa, according to standards definitions (American Society for Testing and Materials, 2019) to no vacuum (i.e.,10^3 and 10^5 Pa) conditions increases the TTF about 3 times. The longest failure resistance was achieved for the tank equipped with an 80-layer MLI under complete loss of vacuum (TTF= 30 min 40 s). In comparison, the shortest TTF (10 min) was observed for a 20-layer MLI at high vacuum conditions (i.e., 0.001 Pa). Although vacuum loss must be prevented in normal operating conditions (it causes a severe drop in insulation performances), simulations of fire scenarios indicate an increase of pressure in the gap may improve the fire resistance of LH_2 tanks featuring MLI systems. Such results are in line with what observed experimentally by Eberwein et al. (2024b) on a combustible MLI. The reasons for this effect can be

understood by analyzing two reference cases: Case A, where the tank features a 20-layer MLI that operates at 0.001 Pa, and Case B, where the 20-layer MLI operates at 10^5 Pa.

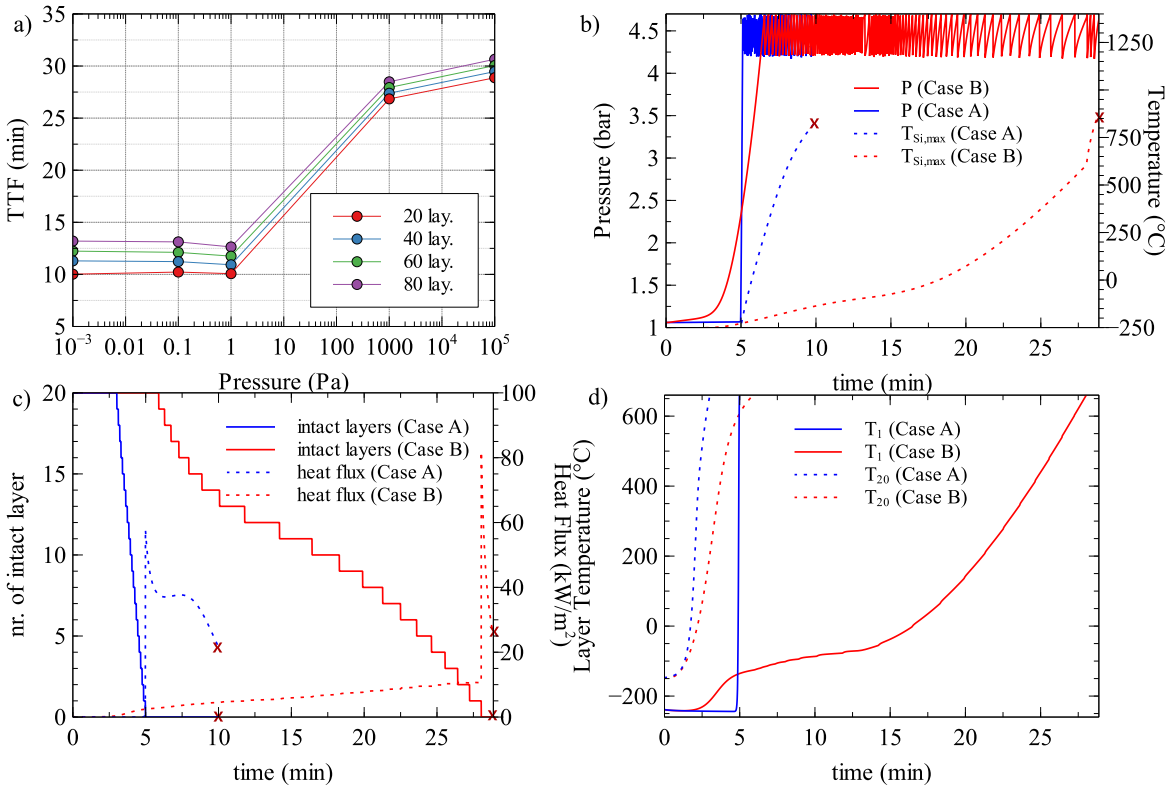

Figure 2. Results of the case studies. TTF: time to mechanical failure; P: tank pressure; Tsi.max: maximum inner shell temperature; T_1: temperature of the MLI layer facing the inner shell wall; T_{20}: temperature of the MLI layer facing the external shell. Case A is referred to a 20-layer MLI operating under 0.001 Pa (blue curves) and Case B to the same MLI but operating at 10^5 Pa (red curves). The crosses indicate the moment of tank failure.

Figure 2b shows the pressure (*P*) within the inner tank (left axis) and the increase in maximum shell temperature ($T_{Si,max}$, right axis) for the two cases. In Case B, the inner shell temperature and pressure rise after an induction time of 2 min 30 s. In Case A, $T_{Si,max}$ and *P* remain at initial values for a longer time after fire ignition (i.e., 5 min) due to higher insulation effectiveness determined by high-vacuum conditions. After this initial phase, Case A presents an abrupt increase in both *P* and $T_{Si,max}$, leading to early PRV activation compared to Case B. From this moment onwards, the PRV chattering occurs together with a constant increase in shell temperature in Case A, culminating with the tank failure at a total exposure time of 10 min. On the contrary, Case B presents a slower temperature and pressure increase in the same period, resulting in a delayed failure of the equipment (30 min 54 s). Such a different behavior arises because the degradation of the MLI layer occurs earlier in Case A than in Case B. This can be observed in Figure 2c, which shows the remaining intact layers (left axis) and the heat fluxes to the inner wall of the tank (right axes) over time for both cases. In Case A, all the MLI layers degrade after 5 min of exposure and the heat flux increases abruptly. In Case B, the degradation progresses more gradually (the complete degradation of the MLI occurs after 28 min) determining a slower rise of the layer temperature (especially of those closer to the inner shell) as can be observed in Figure 2d. This is caused by the increased gaseous heat transfer when the vacuum is lost, which allows each reflective layer to dissipate more heat to the next layer compared to vacuum conditions.

Overall, the simulations demonstrate that, although vacuum loss anticipates the instant of time at which temperature and pressure start to rise within the tank, these increase at a slower rate compared to cases in which the vacuum is preserved, with beneficial effects on the time to failure. This suggests that breaking the vacuum could be considered a mitigating action in case of fire exposure.

4. Conclusions

This study presents an innovative model for estimating the time to failure (TTF) of MLI thermally insulated LH_2 tanks under fire exposure, incorporating MLI thermal degradation mechanisms, PRV action, and a simplified stress analysis. A series of case studies set up to assess the impact of the insulation pressure and the number

of MLI layers on the TTF of typical vehicle-scale tanks revealed that such systems can be severely threatened by fire. The mechanical failure occurred in all the cases analyzed within 10 to 31 minutes of exposure to a hydrocarbon pool fire with a maximum flame temperature of 1100 °C, highlighting a significant challenge in ensuring the integrity of these tanks in such conditions. A comprehensive analysis of the results demonstrated that increasing the number of MLI layers from 20 to 80 prolongs failure resistance by only a few minutes (from 1 to 3 min). In contrast, pressure within the insulation has a significant impact on the TTF. Going from high-vacuum to atmospheric pressure the TTF increases from 10 min to 30 min 40 s for an MLI with 20 reflective layers, due to slower MLI degradation from increased gaseous heat transfer. Thus, in case of fire exposure, breaking the vacuum could represent an effective mitigation measure to delay tank failure. Overall, the findings of the present study provide key insights for optimizing MLI configurations and guiding fire safety standards for hydrogen storage systems.

Acknowledgments

This work is part of the NICOLHy project (No. 101137629) funded by the EU and Clean Hydrogen Partnership. Views and opinions expressed are however those of the authors only and do not necessarily reflect those of the EU or Clean Hydrogen JU. Neither the EU nor the granting authority can be held responsible for them.

References

American Society for Testing and Materials, 2019. Standard Guide for Evacuated Reflective Insulation In Cryogenic Service (ASTM C740/740M-13).

Bell, I.H., Wronski, J., Quoilin, S., Lemort, V., 2014. Pure and Pseudo-pure Fluid Thermophysical Property Evaluation and the Open-Source Thermophysical Property Library CoolProp. Ind. \& Eng. Chem. Res. 53, 2498–2508. https://doi.org/10.1021/ie4033999

Camplese, D., Scarponi, G.E., Chianese, C., Hajhariri, A., Eberwein, R., Otremba, F., Cozzani, V., 2024. Modeling the performance of multilayer insulation in cryogenic tanks undergoing external fire scenarios. Process Saf. Environ. Prot. 186, 1169–1182. https://doi.org/10.1016/j.psep.2024.04.061

Churchill, S.W., Usagi, R., 1972. A general expression for the correlation of rates of transfer and other phenomena. AIChE J. 18, 1121–1128.

Eberwein, R., Hajhariri, A., Camplese, D., Scarponi, G.E., Cozzani, V., Otremba, F., 2024a. Experimental investigation on the behavior of thermal super insulation materials for cryogenic storage tanks in fire incidents. Process Saf. Environ. Prot. 187, 240–248. https://doi.org/10.1016/j.psep.2024.04.131

Eberwein, R., Hajhariri, A., Camplese, D., Scarponi, G.E., Cozzani, V., Otremba, F., 2024b. Experimental Research Of A Tank For A Cryogenic Fluid With A Wall Rupture In A Fire Scenario, in: 15th ISHPMIE. Naples. https://doi.org/10.5281/zenodo.12621001

Edward, L., Filip, L., 2018. Influence of vacuum level on insulation thermal performance for LNG cryogenic road tankers, in: MATEC Web of Conferences. EDP Sciences, p. 1019.

EN 1993-1-2, 2024, Eurocode 3: Design of steel structures. Part 1-2: Structural fire design

EN 1993-1-4, 2006, Eurocode 3: Design of steel structures - General rules. Supplementary rules for stainless steels

ISO 21013-3, 2016, Cryogenic vessels – Pressure-relief accessories for cryogenic service – Part 3: Sizing and capacity determination

Kunze, K., Kircher, O., 2012. Cryo-compressed hydrogen storage cryogenic cluster day. Oxford, Sept. 28, 2012.

McIntosh, G.E., 1994. Layer by Layer MLI Calculation Using a Separated Mode Equation Advances in Cryogenic Engineering, in: Kittel, P. (Ed.), Advances in Cryogenic Engineering. Springer US, Boston, MA, pp. 1683–1690. https://doi.org/10.1007/978-1-4615-2522-6_206

Pehr, K., 1996. Experimental Examinations on the Worst Case Behavior of LH2/LNG Tanks for Passenger Cars, in: Proceedings of the 11th World Hydrogen Energy Conference, Stuttgart, Germany. pp. 2169–2186.

Preuster, P., Alekseev, A., Wasserscheid, P., 2017. Hydrogen Storage Technologies for Future Energy Systems. Annu. Rev. Chem. Biomol. Eng. 8, 445–471. https://doi.org/10.1146/annurev-chembioeng-060816-101334

Schiaroli, A., Scarponi, G.E., Antonioni, G., Cozzani, V., 2024. Hazard footprint of alternative fuel storage concepts for hydrogen-powered urban buses. Int. J. Hydrogen Energy 50, 1430–1442. https://doi.org/10.1016/j.ijhydene.2023.11.104

Van Den Bosh, C.J.H., Weterings, R., 2005. TNO Yellow Book, Methods for the calculation of physical effects, Sdu Uitgevers.

van Wingerden, K., Kluge, M., Habib, A.K., Ustolin, F., Paltrinieri, N., 2022. Medium-scale Tests to Investigate the Possibility and Effects of BLEVEs of Storage Vessels Containing Liquified Hydrogen. Chem. Eng. Trans. 90, 547–552. https://doi.org/10.3303/CET2290092

Wang, L., Li, Y., Zhang, F., Xie, F., Ma, Y., 2016. Correlations for calculating heat transfer of hydrogen pool boiling. Int. J. Hydrogen Energy 41, 17118–17131. https://doi.org/10.1016/j.ijhydene.2016.06.254